

The reaction between propene and hydroxyl†

Judit Zádor,* Ahren W. Jasper and James A. Miller*

Received 31st July 2009, Accepted 17th September 2009

First published as an Advance Article on the web 13th October 2009

DOI: 10.1039/b915707g

Stationary points on the C₃H₇O potential energy surface relevant to the title reaction are calculated employing RQCISD(T)/cc-pV ∞ Z//B3LYP/6-311++G(d,p) quantum chemical calculations. Rate coefficients at 50–3000 K temperature and from zero to infinite pressure are calculated using an RRKM-based multiwell master equation. Due to the topography of the entrance channel an effective two-transition-state model is used to calculate accurate association rate coefficients. Our calculations are in excellent agreement with the available experimental data. We predict ~5% vinyl alcohol branching above 1000 K, the allyl radical formation being the main channel at high temperatures.

Introduction

The fate of alkenes is of general interest in both atmospheric and combustion chemistry. Propene is of particular interest as a prototype alkene fuel, as it may be expected to exhibit a richer combustion chemistry than ethene and yet is simple enough to permit a detailed theoretical analysis. Propene is an important intermediate in many combustion mechanisms and can be found in practical fuels in small amounts. In the atmosphere propene is emitted directly from anthropogenic or natural sources, and it is also formed *via* the photolysis of larger aldehydes and ketones. The reaction of propene with OH is its major reaction pathway under typical atmospheric or combustion conditions.

The dominant reaction channels of the propene + OH reaction change with temperature and pressure, which is typical of olefin–hydroxyl radical reactions. Below ~500 K, OH adds to the double bond in propene, and the initial adduct is stabilized even at moderate pressures. The experimentally observed negative temperature dependence in this range is in accordance with calculated features of the potential energy surface (PES) in the entrance channel. Quantum chemical calculations^{1–7} predict a barrierless entrance channel into a van der Waals well, which then may proceed to the C₃H₇O adducts *via* a low barrier. Although the previous theoretical studies predict qualitatively similar features of the potential energy surface in the entrance channel, significant quantitative differences were reported. The overall kinetics is expected to be extremely sensitive to details of the potential energy surface in this region.

Above ~700 K, H-atom abstraction is the dominant decay mechanism, as observed experimentally.^{8–10} Addition is a minor product channel due to fast backdissociation of the initial adducts. A small fraction of the reactants form non-abstraction bimolecular products, which can also be detected

experimentally. Abstraction shows a positive temperature dependence and readily leads to the formation of allyl radicals, one of the resonance-stabilized radicals that contribute to soot formation in flames.^{11–14} Among other bimolecular products, the reaction can lead to the formation of vinyl alcohol, a common but only recently discovered intermediate in flames.^{15,16}

The propene + OH reaction is also important in understanding the OH-initiated oxidation of 1- and 2-propanol,^{17,18} where dehydration of the alcohol takes place *via* the unimolecular dissociation of the β -hydroxypropyl radicals at elevated temperatures:



The interference from the unimolecular decomposition becomes relevant above ~500 K, and it is crucial to know the rate coefficients of (R1) and (R2) to evaluate both OH + propanol and bulk propanol combustion experiments.

The overall rate coefficient of the propene + OH reaction has been extensively measured experimentally^{8,9,19–34} and reported in data evaluations^{10,28,35,36} between 58 K and 1210 K. It is important to note that experimental data is lacking between approximately 500 and 700 K, because the reaction mechanism in this temperature region involves both addition and abstraction, and therefore, simple pseudo-first-order experimental strategies fail. Experimental data on product branching fractions include only a low-pressure mass-spectrometric study.³⁷

There have been several previous theoretical calculations of the C₃H₇O potential-energy surface.^{1–4,7} Two recent papers report theoretical calculations of the rate coefficient of the propene + OH reaction.^{5,6} Huynh *et al.*⁶ calculated rate coefficients for temperatures above 500 K using an RRKM-based master equation (ME) methodology and obtained the rate coefficients from the time-evolution of the species (*i.e.* the initial-rate method³⁸). Zhou *et al.*⁵ treated the entrance channel for addition with a two-transition-state model, applying variable-reaction-coordinate transition state theory (VRC-TST) with a model potential energy surface for the loose, outer transition state, and conventional TST for the

Combustion Research Facility, Sandia National Laboratories, MS 9055, Livermore, CA 94551-0969, USA.
E-mail: jamille@sandia.gov; jzador@sandia.gov;
Fax: +1 (1)925 294 2276

† Electronic supplementary information (ESI) available: Modified Arrhenius fits in CHEMKIN format. See DOI: 10.1039/b915707g

tight, inner transition state. They calculated rate coefficients for 200–3000 K based on the ME methodology implemented in the Variflex code version 1.0. Also, Izsák *et al.*⁷ calculated the energetics of the entrance channel for the propene + OH reaction and carried out a conventional TST calculation for some aspects of the kinetics.

In this work we calculate the overall rate coefficient and branching fractions for 50–3000 K and a wide range of pressures using high-level *ab initio* methods and RRKM-based multiwell master equation methods. We use direct VRC-TST for the barrierless entrance channel, a method which does not require a model PES. To combine the outer and inner transition states, an effective two-transition-state model is used. We obtain rate coefficients from the eigenvectors and eigenvalues of the ME, a method applicable even at high temperatures. Our overall methodology was previously used by Greenwald *et al.*^{39,40} and Senosian *et al.*⁴¹ to characterize the reactions of OH with ethylene and isoprene.

Construction of the PES

Optimized geometries, frequencies, relaxed internal rotational potentials, and energies of the stable complexes and saddle points along the intrinsic reaction coordinate (IRC) were calculated on the C₃H₇O potential energy surface. Geometry optimizations and IRC scans were performed with density functional theory (DFT) calculations using the B3LYP functional and the d,p-polarized split valence 6-311 + +G(d,p) Gaussian basis set. In all cases, lowest energy conformers were determined in a systematic manner, *i.e.* we calculated the potential along all dihedral angles where the rotation is possible around a single bond, and selected the global minimum of these structures. We were unable to locate a saddle point using the DFT method in only a few instances, most significantly the inner transition states leading to the adducts were not present on the B3LYP PES. Based on previous studies,^{39,40} we expect the predicted rate coefficients to be highly sensitive to the potential energy surface in this region. Therefore, in this case three alternative methods were applied for the computation of the optimized geometries and frequencies: (1) the second-order Møller–Plesset perturbation theory (MP2) with the d,p-polarized split valence 6-311 + +G(d,p) Gaussian basis set; (2) the quadratic configuration interaction with single and double excitations (QCISD) using the same basis set; and (3) the multireference second order perturbation theory (CASPT2) method with an active space consisting of 3 electrons in 3 orbitals and using Dunning’s augmented correlation consistent basis set, aug-cc-pVDZ.

For the computation of accurate single point energies of open-shell molecules we used the restricted open-shell quadratic-configuration-interaction method with single and double excitations and correction for triple excitations, ROHF-RQCISD(T), with the cc-pVnZ basis sets, $n = (T, Q)$, extrapolated to the infinite basis set limit cc-pV ∞ Z; the RHF-RQCISD(T)/cc-pV ∞ Z method was applied for closed-shell molecules.⁴² For the extrapolation to the infinite-basis-set limit the asymptotic form suggested by Martin⁴² and by Feller and Dixon,⁴³ was used: $E_\infty = E_{l_{\max}} - B/(l_{\max} + 1)^4$,

where E_∞ is the infinite basis-set energy, B is a least-square fit parameter (not needed for the calculation) and l_{\max} is the maximum component of angular momentum in the cc-pVnZ basis set, which is 3 and 4 for the triple ($n = 3$) and quadrupole ($n = 4$) basis sets, respectively. The CCSD(T) method was previously tested⁴⁴ against a database of well-known barrier heights⁴⁵ and was found to be perform slightly worse than the QCISD(T) method. The QCISD(T) method is equivalent to a slightly truncated CCSD(T) method, and its somewhat better performance is probably due to cancellations of errors. The CCSD(T) method is not considered further in the present work. The DFT, MP2 and QCISD calculations were performed using the *Gaussian 03* suite of programs,⁴⁶ and the other quantum chemical calculations employed the *MOLPRO* package.⁴⁷

Calculation of rate coefficients

The RRKM/ME methodology developed by Miller and Klippenstein^{38,48,49} was used to determine phenomenological rate coefficients. The 1D ME can be represented in a matrix form:

$$\frac{d|w(t)\rangle}{dt} = \mathbf{G}|w(t)\rangle \quad (1)$$

where matrix \mathbf{G} describes the chemical exchange between the various wells and also the energy transfer during collisions, while $|w(t)\rangle$ contains the unknown populations. The rate coefficients were calculated using the eigenvalue–eigenvector based solution of eqn (1).

Greenwald *et al.*³⁹ found that in the ethene + OH system, tunneling through the inner saddle point is significant only below ~ 200 K, where the outer, barrierless transition state dominates. Therefore, tunneling is expected to have only a small effect on the calculated addition rate coefficients. Nevertheless, asymmetric Eckart barriers were used to model tunneling in 1D through saddle points. In the same study it was also found that using hindered rotors instead of harmonic oscillators gave a very significant correction to the calculated rate coefficients. In this work the low-frequency torsional modes were treated as hindered rotors using the Pitzer–Gwinn approach⁵⁰ applied to state densities. The hindering potentials were determined for every geometry around every possible dihedral angle by fitting Fourier series with six sine and six cosine terms to the B3LYP/6-311 + +G(d,p) energies along the relaxed internal rotation. Collisional energy transfer was approximated by a simple exponential-down model, where the average downward transfer parameter $\langle \Delta E_d \rangle$ was assumed to be temperature-dependent with the form $200 \times (T/300 \text{ K})^{0.85} \text{ cm}^{-1}$. This model and these parameters were previously used to study the kinetics of the reaction of OH with ethylene.⁴¹ Lennard-Jones parameters for the C₃H₇O isomers were taken as that of propanol,⁵¹ $\sigma = 4.459 \text{ \AA}$, $\epsilon/k_B = 576.7 \text{ K}$. The multiwell ME calculations were carried out with the VARIFLEX program package, version 2.0.⁵² The main difference between VARIFLEX 1.0 and the later versions is that the ME methodology described in the papers of Miller and Klippenstein^{38,48,49} is included. Therefore, the kinetic information can be extracted from systems with more than one chemically significant eigenvalue.

The microcanonical, J -resolved (J is the total angular momentum) number of states for the barrierless entrance to the van der Waals well was calculated variationally using direct VRC-TST.^{53,54} The distance between the propene center of mass and the OH center of mass (practically the O atom) was taken as a reaction coordinate and allowed to vary between 4.2 and 10.0 Å. The potential energy was evaluated using the state averaged CASPT2(5e,4o)/aug-cc-pVDZ method, where the active orbitals are the bonding and antibonding π orbital of the C–C double bond, the π orbital of the OH radical and the radical orbital, and two electronic states were included. Our unpublished results show that using non-augmented basis-sets for the C–O potential leads to significant errors and the difference between the energies calculated with double and triple zeta basis sets is large. However, when using the augmented versions of the basis sets the correction becomes negligible. Therefore, no basis set correction was employed in this work. The effect of geometry relaxation on the computed rates was determined to be negligible as the geometries of the isolated fragments and the van der Waals complex are very close; the O–H bond length changes by 0.006 Å and the C–C bond length changes by 0.003 Å. This is also supported by the findings of Greenwald *et al.*³⁹ for the ethene + OH reaction, where geometry relaxation effects were found to be <10% for the inner transition state; these effects are expected to be even smaller for the outer one. The inner transition states were not treated variationally, as expected corrections from this treatment are small.³⁹ The VRC-TST calculations were carried out using the VaReCoF code.⁵⁵ This program determines the microcanonical J -resolved transitional number of states throughout a set of dividing surfaces, defined as spheres of increasing radius in our case, by sampling a large number of quasi-randomly selected orientations of the fragments.

The overall rate coefficient at very low temperatures is controlled by the long-range dynamical bottleneck associated with the outer, barrierless transition state, while at higher temperatures it is controlled by the inner transition states associated with the saddle points for each addition channel. The overall effect of the two types of controlling bottlenecks at an arbitrary temperature can be determined by a generalization of the two-transition-state model,^{56–60} applied to three transition states in our case. This model assumes a collision-free environment for the van der Waals complex, and therefore conserves E and J between the two transition-state regions. The flux at the van der Waals minimum is much greater than the flux at any one of the transition states, because the van der Waals well is well below the tight transition states, and because the harmonic frequencies at this geometry are also lower.

It was shown by Greenwald *et al.*^{39,40} that any steady-state assumption for the weakly bound complex has to be implemented at the microcanonical, J -resolved level, because the shallowness of the corresponding well prevents thermal distributions to be established.

The overall flux through the inner transition states, $N_{\text{inner}}^{\neq}(E, J)$, is simply the sum of the fluxes through the individual inner transition states:

$$N_{\text{inner}}^{\neq}(E, J) = N_t^{\neq}(E, J) + N_c^{\neq}(E, J) \quad (2)$$

where $N_t^{\neq}(E, J)$ and $N_c^{\neq}(E, J)$ are the E and J resolved number of states for the inner transition state on the terminal and the central carbon atoms, respectively. Combining $N_{\text{inner}}^{\neq}(E, J)$ with the outer transition state flux the effective overall flux is:

$$\frac{1}{N_{\text{effective}}^{\neq}(E, J)} = \frac{1}{N_{\text{outer}}^{\neq}(E, J)} + \frac{1}{N_{\text{inner}}^{\neq}(E, J)} - \frac{1}{N_{\text{max}}} \quad (3)$$

where N_{max} is the maximum flux between the inner and outer transition states. Since N_{max} is much greater than the fluxes at the transition states, the last term can be neglected.

The branching ratio to the individual channels is simply $N_t^{\neq}(E, J)/N_{\text{inner}}^{\neq}(E, J)$ and $N_c^{\neq}(E, J)/N_{\text{inner}}^{\neq}(E, J)$, which yields the following equations for the effective transition state number of states for the addition to the terminal and the central carbon atoms, $N_{t,\text{effective}}^{\neq}(E, J)$ and $N_{c,\text{effective}}^{\neq}(E, J)$, respectively:

$$N_{i,\text{effective}}^{\neq}(E, J) = \frac{N_i^{\neq}(E, J) \times N_{\text{outer}}^{\neq}(E, J)}{N_{\text{outer}}^{\neq}(E, J) + N_{\text{inner}}^{\neq}(E, J)}, \quad i = t \text{ or } c \quad (4)$$

The strong coupling between the nuclear rotation and the electronic spin of the OH radical further complicates the calculation of the effective rate coefficient. At low temperatures the rovibronic partition function of the free OH is evaluated conventionally (*i.e.* electronically decoupled), since $N_{\text{outer}}^{\neq}(E, J)$ is calculated that way as well. At higher temperatures, however, where the inner transition state dominates, the coupled, quantized rovibronic partition function for the free OH radical is needed. In order to correct for this effect at intermediate temperatures at the canonical level, we used the *ad hoc* correction f suggested by Greenwald *et al.*³⁹

$$f = \frac{k'_{\text{inner}}(T) \times k_{\text{outer}}(T)}{k'_{\text{inner}}(T) + k_{\text{outer}}(T)} \times \left(\frac{k_{\text{inner}}(T) \times k_{\text{outer}}(T)}{k_{\text{inner}}(T) + k_{\text{outer}}(T)} \right)^{-1} \quad (5)$$

where $k_{\text{inner}}(T)$ and $k_{\text{outer}}(T)$ are evaluated with the decoupled partition functions and $k'_{\text{inner}}(T)$ is evaluated with the correctly coupled quantized OH partition function. The correction factor f is always smaller than 1 and has a minimum around 250 K (0.86). Details of determining the uncoupled and coupled partition functions for OH are presented in the Appendix.

The spin-orbit coupling of the OH radical at the inner transition state is ignored, because it is much smaller than at infinite separation. The coupling only has an effect on the interaction energy, which is thus increased by 70 cm⁻¹.

Results and discussion

The C₃H₇O potential energy surface

The main features and the corresponding geometries of the underlying potential energy surface are discussed in the literature;^{1–3,5,6} therefore only a brief description is given here. Addition of the OH radical can take place on the terminal (Fig. 1) carbon atom, forming 1-hydroxy-prop-2-yl, or on the secondary carbon atom (Fig. 2) forming 2-hydroxy-prop-1-yl. These complexes can be collisionally stabilized and/or undergo isomerization and dissociation leading to various bimolecular products. The OH radical can also abstract an H atom directly (Fig. 3) forming water and an open shell species.

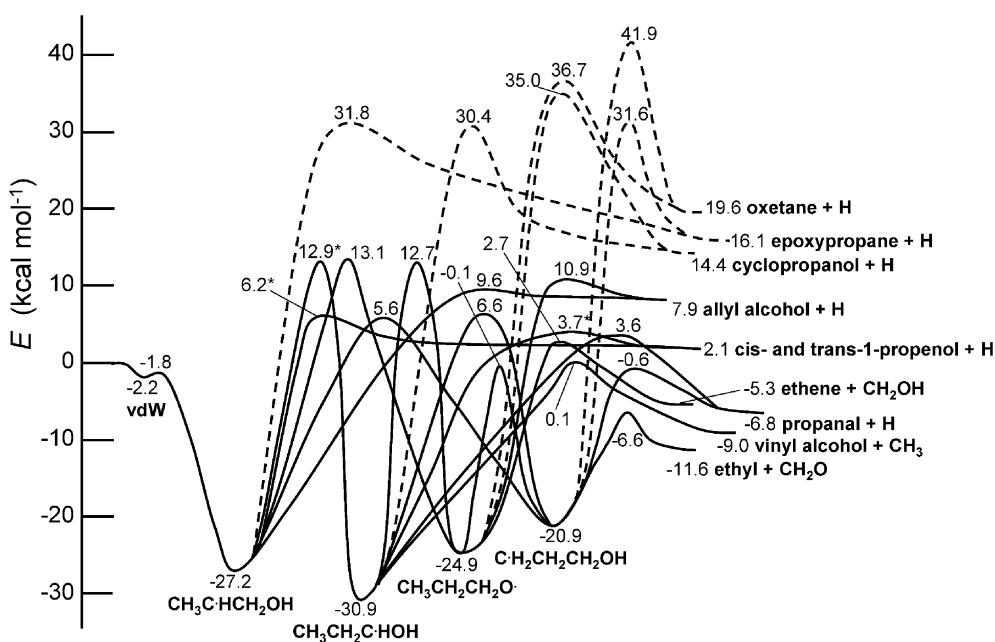


Fig. 1 The C_3H_7O potential energy surface (including ZPE) for the terminal addition of the OH radical. Most of the energies are calculated using RQCISD(T)/cc-pV ∞ Z//B3LYP/6-311 + G(d,p); for details see text. *: there are two different barriers, one for the *cis* and one for the *trans* isomer. For clarity, only the lower one is shown. Channels with barriers above 20 kcal mol^{-1} are marked with a dashed line.

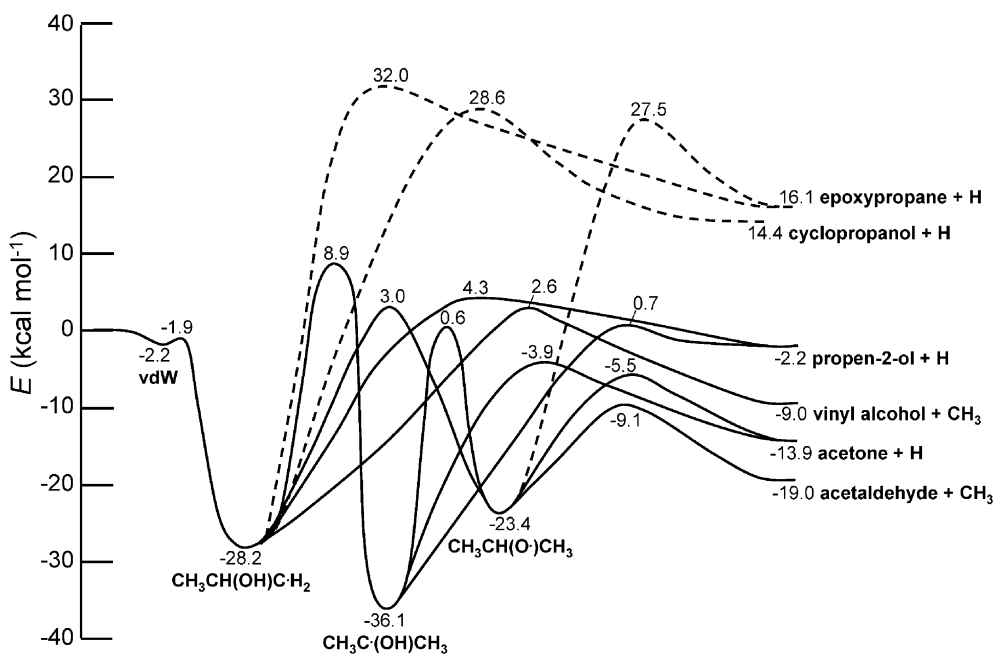


Fig. 2 The C_3H_7O potential energy surface (including ZPE) for the central addition of the OH radical. Most of the energies are calculated using RQCISD(T)/cc-pV ∞ Z//B3LYP/6-311 + G(d,p); for details see text. Channels with barriers above 20 kcal mol^{-1} are marked with a dashed line.

Both addition channels proceed *via* a common van der Waals well, **vdW**. The structure of the **vdW** is very similar to that in the $C_2H_4 + OH$ system: the OH bond is approximately perpendicular to the plane of the propene and the H atom is pointing towards the middle point of the C–C double bond. In Fig. 4 a constrained PES scan in the region of the outer TS is presented. In these constrained calculations, the OH molecule, with the H atom inward, was always oriented toward the center of mass of the propene molecule. The origin of Fig. 4

indicates the center of mass of propene, and the three carbon atoms of propene lie in the plane perpendicular to the *xy*-plane, with the double bond placed along the *x*-axis and the methyl group toward negative values of *x*. It can be seen that the PES is very shallow perpendicular to the reaction coordinate.

Szöri *et al.*^{1,7} found that the abstraction of the allylic H proceeds *via* the same complex, and they did not find any other van der Waals complexes of propene and OH.

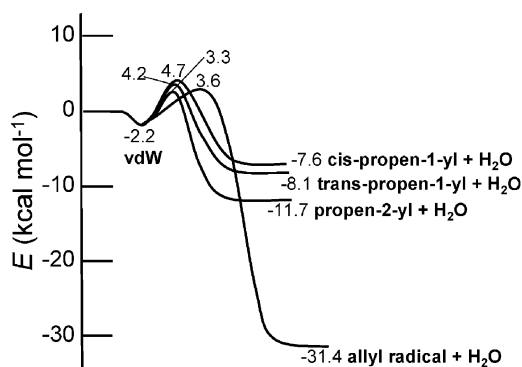


Fig. 3 The C_3H_7O potential energy surface (including ZPE) for the abstraction channels. Most of the energies are calculated using RQCISD(T)/cc-pV ∞ Z//B3LYP/6-311 + G(d,p); for details see text.

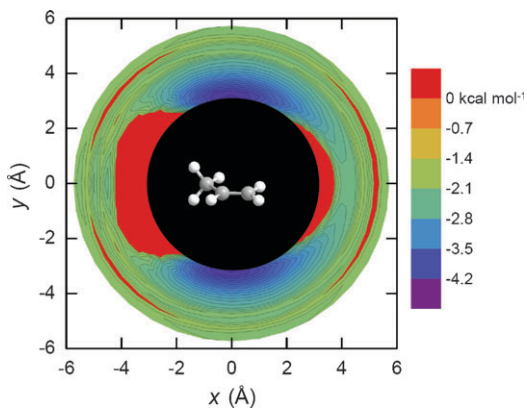


Fig. 4 2D slice of the PES in the region of the outer transition state. Energies are calculated outside the black area only. For more details see text.

The abstraction of the other hydrogen atoms is very likely to proceed also through the same complex. We did not attempt, however, to prove these connections since they have no effect on our calculated rate coefficients.

The calculated barrier height of the allylic H-abstraction channel shows a notable scatter in the literature.^{1,3} However, even the lowest calculated barrier height is higher than the entrance channel. It means that even at very low temperatures the association rate is determined by the inner transition state. Therefore, in this work the transition states related to direct H-abstraction are treated as tight transition states, without accounting for contributions from the outer transition state ($N_{\text{abstraction}}^{\ddagger} \ll N_{\text{outer}}^{\ddagger}$).

The inner transition states $\text{vdW} \leftrightarrow \text{CH}_3\text{C}\cdot\text{HCH}_2\text{OH}$ and $\text{vdW} \leftrightarrow \text{CH}_3\text{CH}(\text{OH})\text{C}\cdot\text{H}_2$ were not found using the B3LYP density functional method. Systematic scanning of the B3LYP surface found no maximum on the surface, except for a very small one (<0.2 kcal mol $^{-1}$, 1 cal = 4.184 J) at ~ 3 Å, which does not correspond to the transition state sought. Using other quantum chemical methods we were able to locate the geometries of the inner transition state and in this work we use the ones obtained by CASPT2(3e,3o)/aug-cc-pVDZ. We also located these structures using MP2/6-311 + G(d,p) and QCISD/6-311 + G(d,p) levels of theory. The main geometric parameters, the imaginary frequencies and the

ROHF-RQCISD(T)/cc-pV ∞ Z energies for these geometries, can be found in Table 1. The three geometries are slightly different, e.g. in the CASPT2 structure the OH is somewhat (~ 0.3 Å) further from the double bond. The energies shown in Fig. 1 and 2 for these saddle points (-1.8 and -1.9 kcal mol $^{-1}$) were obtained at the ROHF-RQCISD(T)/cc-pV ∞ Z//CASPT2(3e,3o)/aug-VDZ level of theory. All of the high-level single-point energy calculations suggest that the barrier heights leading to the two different adducts (terminal and non-terminal) are very similar.

When the OH adds to the terminal carbon atom (Fig. 1), the most probable bimolecular products are *cis*- and *trans*-1-propenol + H, propanal + H and ethyl + CH $_2$ O. Although the exit channels leading to ethene + CH $_2$ OH and vinyl alcohol + CH $_3$ are also low, the preceding isomerization steps have relatively high barriers. Therefore, low yields of these products are expected. However, vinyl alcohol can also be formed by addition to the central carbon atom, where there is no isomerization step involved.

The lowest energy channel in the central addition case (Fig. 2) leads to the formation of vinyl alcohol and a methyl group. The other low-energy channels lead to the formation of acetone + H and acetaldehyde + CH $_3$. In both the terminal and central cases the transition state energies for cyclic compounds are very high on the PES. Note that the transition-state structure $\text{CH}_3\text{C}(\text{OH})\text{CH}_3 \leftrightarrow \text{propen-2-ol} + \text{H}$ could not be located by our DFT method; instead, we used MP2/6-311 + G(d,p).

The direct H-abstraction channels (Fig. 3) can lead to *cis*- and *trans*-propen-1-yl, propen-2-yl and allyl radicals, always with an H $_2$ O molecule. The barriers leading to these products are significantly higher than the entrance channel: 4.2, 4.7, 3.3 and 2.9 kcal mol $^{-1}$, respectively. This makes the two-transition-state treatment of these reaction channels unnecessary, since at the temperatures of interest here the reaction is controlled by these inner barriers. The allylic transition state was found by MP2/6-311 + G(d,p), but not by B3LYP/6-311 + G(d,p), a situation similar to the inner transition states of the addition channels. In the extensive study of Szőri *et al.*,^{1,7} the barrier for the allylic abstraction was found to be 0.74 kcal mol $^{-1}$ (using QCISD(T)/6-311 + G(3df,2p)//CCSD/6-31G(d) method), which is significantly lower than the one computed here (2.9 kcal mol $^{-1}$); our result is in reasonable agreement with that of Huyhn *et al.*⁶ (1.6 kcal mol $^{-1}$) and Zhou *et al.*⁵ (2.6 kcal mol $^{-1}$). Although the reason for the discrepancy between our value and that of Szőri *et al.* is not clear, the good agreement of our calculated H-abstraction rate coefficient with the experimental values suggest that our barrier heights are reasonable.

Szőri *et al.*^{1,7} found two transition states for the allylic abstraction, and they assigned two channels to them. The “direct” channel is not connected to the van der Waals well, while the “indirect” channel proceeds *via* the van der Waals well. We found the two corresponding transition states to be rotamers of each other (also suggested by Szőri *et al.*¹) and separated by a small second-order saddle point of 0.8 kcal mol $^{-1}$. In our kinetic analysis, therefore, the two channels are treated as one, and we include the corresponding hindering potential when calculating the state densities.

Table 1 Selected geometric and energetic properties of the two inner transition states, obtained by three different methods

Geometry	$d(\text{C}-\text{O})/\text{\AA}$	O-C-C/deg	Imaginary frequency/cm ⁻¹	ZPE/kcal mol ⁻¹	ROHF-RQCISD(T)/cc-pV ∞ Z energy including ZPE/kcal mol ⁻¹
vdW \leftrightarrow terminal addition					
MP2/6-311++G(d,p)	2.07	96.8	541 <i>i</i>	58.4	-0.5
CASPT2(3e,3o)/aug-VDZ	2.40	92.8	141 <i>i</i>	56.2	-1.8
QCISD/6-311++G(d,p)	2.15	98.3	324 <i>i</i>	57.3	-1.1
vdW \leftrightarrow central addition					
MP2/6-311++G(d,p)	2.07	99.9	537 <i>i</i>	58.2	-0.5
CASPT2(3e,3o)/aug-VDZ	2.39	91.4	134 <i>i</i>	56.4	-1.9
QCISD/6-311++G(d,p)	2.14	95.7	334 <i>i</i>	57.2	-1.0

The Q1 diagnostic of Lee *et al.*^{61,62} indicates multireference character of the wave function. For most of our stationary points the value of Q1 is small (<0.02), meaning that using a single-reference method is appropriate. For the transition states **vdW** \leftrightarrow CH₃C-HCH₂OH, **vdW** \leftrightarrow CH₃CH(OH)C-H₂, **vdW** \leftrightarrow C₃H₅ + H₂O the diagnostic is higher (0.026–0.028) indicating higher uncertainty in these ROHF-RQCISD(T) energies.

Temperature and pressure dependent kinetics between 50 K and 600 K

In this temperature range, addition is the dominant pathway. Fig. 5 shows our calculated high-pressure limit rate coefficient for 50–600 K along with the available direct experimental data,^{8,19,22,25–28,30} data evaluation³⁶ and the calculations of Zhou *et al.*⁵ This Figure also shows our calculated association rate constants with effect of either the outer transition state or the inner transition states neglected. We also present the theoretical results of Georgievskii and Klippenstein.⁶³ They obtained association rates based on their long-range transition state theory analytical formulas. The various terms corresponding to dipole-dipole ($4.20 \times 10^{-10} \times T^{-1/6}$ cm³ molecule⁻¹ s⁻¹), dipole-quadrupole (2.97×10^{-10} cm³ molecule⁻¹ s⁻¹), dipole-induced dipole ($1.13 \times 10^{-10} \times T^{1/6}$ cm³ molecule⁻¹ s⁻¹) and dispersion interaction ($1.95 \times 10^{-10} \times T^{1/6}$ cm³ molecule⁻¹ s⁻¹) are plotted as a function of temperature below 100 K. The 58 K calculated rate coefficient (4.80×10^{-10} cm³ molecule⁻¹ s⁻¹) is also shown, which accounts for the joint effect of all four interaction types. Note that the low temperature rates due to the various components of the long range forces are not additive.

When the calculated barrier heights for the inner transition states of (-1.8 kcal mol⁻¹ and -1.9 kcal mol⁻¹) were used, the predicted addition rate coefficient is low by a factor of ~ 4 compared to the room temperature experimental value of Tully and Goldsmith⁸ (2.74×10^{-10} cm³ molecule⁻¹ s⁻¹ at 293 K). In order to improve agreement at this temperature, both transition-state energies are lowered to -2.5 kcal mol⁻¹. This accords with the C₂H₄ + OH case,³⁹ and the isoprene + OH case,⁴⁰ where the TS energies had to be lowered by 1.0 and 0.8 kcal mol⁻¹, respectively, relative to the “best” high-level *ab initio* value. Note that the well depth of the van der Waals well is also uncertain to some extent, but it was found to be a minimum with every method used in this work. Therefore, we can safely assume that **vdW** is below the inner transition state; its actual well-depth is immaterial for our calculations.

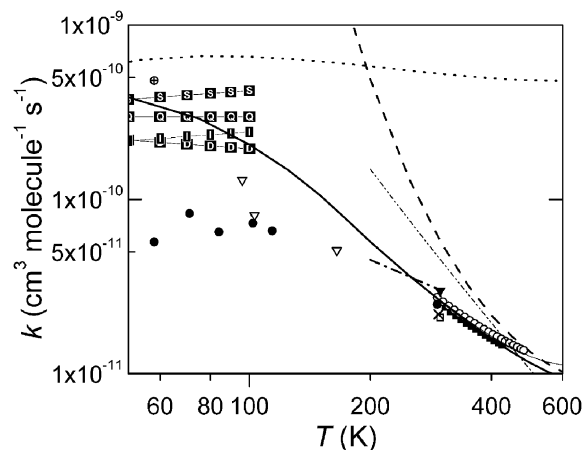


Fig. 5 Comparison of the experimental and calculated high-pressure limiting rate coefficients between 50 and 600 K. Thick solid line: calculated value using the microcanonical, *J*-resolved two-transition-state approach, including the rovibronic correction (eqn (5)). Thin solid line: the same but also including the small contribution from the H-abstraction channels. Dashed line: calculated rate coefficient using the inner transition-state only. Dotted line: calculated rate coefficient using the outer transition-state only. Thin dash-dotted line: calculated rate coefficient of Zhou *et al.*⁵ The letters show the contributions from the various interaction potentials calculated by Georgievskii and Klippenstein.⁶³ D: dipole-dipole interaction; Q: dipole-quadrupole interaction; I: dipole-induced dipole interaction; S: dispersion interaction. / Rate coefficient obtained by the combined effect of D, Q, I and S potentials.⁶³ ● Spangenberg *et al.*;¹⁹ ▽ Vakhtin *et al.*;^{25,26} ○ Tully and Goldsmith;⁸ ■ Atkinson and Pitts;²⁷ ▼ Zellner and Lorenz;²² □ Wallington;³⁰ × Schmidt *et al.*²⁸ Thick dash-dotted line: IUPAC recommendation.³⁶

The literature shows that the calculated energies of these transition states are highly dependent on the level of theory used. Díaz-Acosta *et al.*² and Alvarez-Idaboy *et al.*³ obtained -1.8 , -0.4 and -0.3 kcal mol⁻¹ relative energies for the depth of the van der Waals well and the height of the saddle point barriers, respectively, using the PMP4(SDTQ)/6-311+G**//MP2/6-311G** method and including the zero point energies (ZPE). El-Nahas *et al.*⁴ calculated the barrier heights for the terminal and central addition to be -1.31 and -1.08 kcal mol⁻¹, respectively, using the PMP2/aug-cc-pVTZ//MP2/6-311+G(2d,p) method and including ZPE. Huynh *et al.*⁶ suggest $+1.5$ kcal mol⁻¹ ZPE corrected values for both addition barriers at the CCSD(T)/cc-pVDZ//B3LYP/cc-pVTZ level of theory and -2.4 kcal mol⁻¹ for the depth of the van der Waals well. Zhou *et al.*⁵ found the barrier heights to

be -1.4 and -1.1 kcal mol $^{-1}$ at the PMP2/aug-cc-PVQZ//MP2/cc-PVTZ level, whereas the well depth is -2.6 kcal mol $^{-1}$. Izsák *et al.*⁷ give the standard (298.15 K) enthalpies for the addition channels using UCCSD(T)/CBS//UCCSD(T)/cc-pVTZ level of theory, which are -2.37 kcal mol $^{-1}$ and -2.35 kcal mol $^{-1}$ for the central and terminal case, respectively. It is in reasonable agreement with our respective MP2 (-1.42 kcal mol $^{-1}$ and -1.47 kcal mol $^{-1}$) and QCISD (-1.91 kcal mol $^{-1}$ and -1.93 kcal mol $^{-1}$) standard enthalpy values.

Note that, due to the uncertainties in the calculated barrier heights and in the absence of clear experimental evidence, we are not in a position to change the two barrier heights for the terminal and central addition independently of each other. However, almost all of the theoretical works on propene + OH show that the energies of the two inner barriers are very close to each other.

When considered independently, the inner and the outer transition state rate coefficients are equal to one another at 195 K. Using the effective two-transition-state model, the effective J -resolved, microcanonical rate coefficient at 195 K is $\sim 1/10$ the value of the individual values. Note that using a simpler two-transition-state model at the canonical level would predict a rate coefficient reduction of only $\frac{1}{2}$ at 195 K and would therefore introduce considerable error. At 300 K the effective rate coefficient is 47% of the rate coefficient one would obtain by considering the inner transition states only. This is in line with the trend of ethene³⁹ and isoprene,⁴⁰ where this effect is 30% and 62% at 300 K, respectively. Conversely, the inner transition states lower the rate coefficient at 50 K by 40%, resulting in a value below the predictions of long-range transition-state theory. The influence of the outer transition on the overall rate coefficient becomes negligible only above 600 K.

The abstraction channels start to play a minor, but detectable role above 300 K. In Fig. 5 we show the effective rate coefficient including these channels. At 300 K abstraction makes up $< 1\%$ of total products, while at 600 K it contributes $\sim 15\%$ of the overall rate coefficient; non-abstraction bimolecular channels are negligible. Neglecting the abstraction channels would have a significant effect on the temperature dependence of the predicted rate coefficient. Including these channels gives a remarkably good agreement between theory and the experimental values of Tully and Goldsmith.⁸

We have anchored our 293 K value to the values of Tully and Goldsmith instead of the recommendation of Atkinson.³⁶ That evaluation uses a Troe-type fall-off analysis and suggests 5–6% decrease in the rate coefficient at 760 Torr (1 Torr = 1.33×10^{-3} Torr) compared to the high-pressure limit ($F = 0.5$ and $T^* = 430$ K). Our master equation calculations show, however, that the decrease is less than 1% at 300 K and 760 Torr.

In spite of the very good agreement with the measured rate coefficients of Tully and Goldsmith⁸ and Atkinson and Pitts²⁷ in the 300–500 K temperature range, our calculated rate coefficients, along with the theoretical predictions of Georgievskii and Klippenstein,⁶³ are significantly higher than the low temperature measurements of Vakhtin *et al.*^{25,26} and Spangenberg *et al.*¹⁹ This difference is especially significant

(factor of 6) at the lowest temperature. The discrepancy can probably be attributed to experimental difficulties and is discussed in previous papers.^{40,63} The experiments of Spangenberg *et al.*¹⁹ are around 0.5 Torr, which is still in the high-pressure limit according to our calculations. This rules out the fall-off behavior as a possible reason for the discrepancy. Spangenberg *et al.*¹⁹ argue for a second turnover temperature at low temperatures, below which the temperature dependence becomes positive again. This behavior is reproduced neither in the case of propene + OH nor in the case of isoprene + OH.⁴⁰

The theoretical results of Zhou *et al.*⁵ disagree with both our results and the experimental data by about a factor of 2 at room temperature and also have different temperature dependence. The reasons of this discrepancy are not clear.

In Fig. 6 the experimental and the calculated pressure dependent rate coefficients are compared at 295 K in Ar and He diluents and at 422 K in He diluent. The experimental values are scaled to our high-pressure limit rate coefficients (also shown in the Figure) to facilitate the comparison of the fall-off behaviour. Adjustments are $< 5\%$ for Klein *et al.*, Ravishankara *et al.* and for Tully and Goldsmith at 422 K, while 18% for the data of Vakhtin *et al.*, and 50% for the experimental values of Zellner and Lorenz. In general, our calculations are in excellent agreement with the experiments. It seems, however, that the measurements of Zellner and Lorenz²² overestimate the extent of the fall-off. The rate coefficient under collisionless conditions is 7.6×10^{-15} cm 3 molecule $^{-1}$ s $^{-1}$ at 295 K and 3.4×10^{-14} cm 3 molecule $^{-1}$ s $^{-1}$ at 422 K.

The kinetics of the C₃H₆ + OH reaction above 600 K

Above ~ 600 K the reaction proceeds *via* H-abstraction as well as *via* addition followed by rearrangement and dissociation. The abstraction reaction is independent of pressure, while the

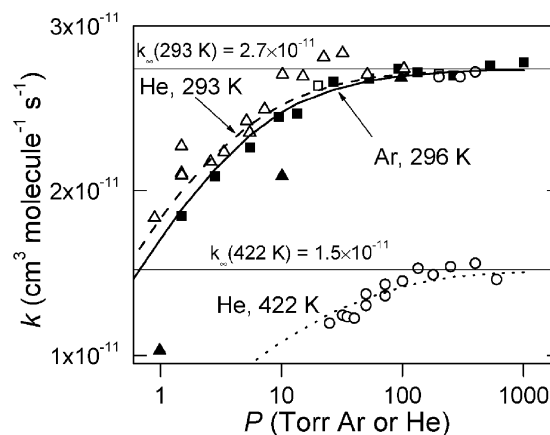


Fig. 6 Pressure dependence of the propene + OH reaction at two different temperatures and with two different bath gases. The calculated values are shown with lines. Solid line: Ar collider, 295 K; dashed line: He collider, 295 K; dotted line: He collider, 422 K. The high-pressure limit is shown with thin horizontal lines. The experimental values are shown with symbols and are scaled to our calculated values to facilitate the comparison of the fall-off behavior. ■ Klein *et al.*,²¹ Ar; ▲ Zellner and Lorenz,²² Ar; □ Ravishankara *et al.*,²⁴ He; ○ Tully and Goldsmith,⁸ He; △ Vakhtin *et al.*,^{25,26} He.

formation of the other bimolecular products is influenced by both pressure and temperature.

In Fig. 7 the rate coefficients of H-abstraction channels are shown along with the data evaluation estimates of Tsang,¹⁰ the available direct experimental data,^{8,9,29} and the other theoretical calculations.^{5,6} Our calculated rate coefficient for the sum of the abstraction and addition/elimination channels supports the experimental values of Tully and Goldsmith.⁸ Furthermore, we are in good agreement with the theoretical calculations of Huynh *et al.*⁶ The recommended estimates of Tsang *et al.*¹⁰ also lie very close to our calculated rate coefficients for propen-1-yl and propen-2-yl. However, the values of Zhou *et al.*⁵ disagree in both the magnitude of the rate coefficient and the branching fractions compared to all other studies. The difference in the branching fraction might be due to the differences in the relative heights of the barriers corresponding to the abstraction reaction. The difference in the overall rate coefficient can be caused by not taking into account key internal-rotor hindering potentials in the calculation.

It is important to distinguish between two seemingly very similar ways of forming non-abstraction bimolecular products. They can be formed by stabilization in the first well followed by isomerization and dissociation (sequential pathway). However, formation of the bimolecular products can also occur without stabilization in the intermediate well(s); this is termed chemical activation or a formally direct pathway. Rate coefficients for the formally direct pathways can be obtained from the eigenvalue-eigenvector based solution of the ME in a straightforward way (for example see ref. 38, 48, 49, 64 and 65).

In the case of the propene + OH reaction it is expected that non-abstraction bimolecular product formation mostly happens through chemical activation pathways. The reason

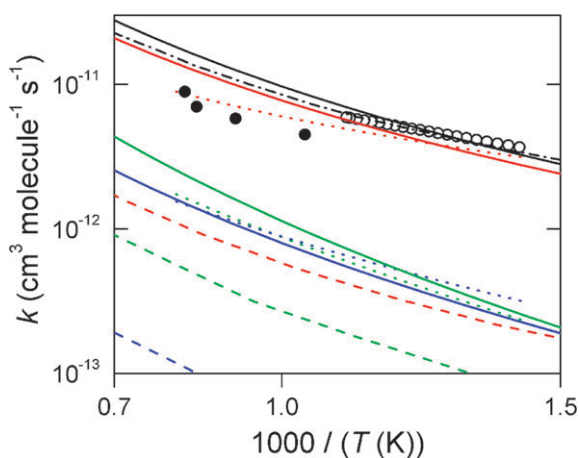


Fig. 7 Arrhenius plot of the high-temperature hydrogen abstraction channels. Red lines: allyl + H₂O; blue lines: propen-1-yl + H₂O; green lines: propen-2-yl. Solid lines: this work; dashed lines: Zhou *et al.*;⁵ dotted lines: recommendations of Tsang;¹⁰ Dash-dotted lines: calculated, overall abstraction rate coefficient, Huynh *et al.*;⁶ black solid line: high-pressure limiting rate coefficient for abstraction and bimolecular product formation, this work; ○: experimental value of Tully and Goldsmith;⁸ ●: experimental value of Smith *et al.*⁹

for this is the relatively high exit barriers from the initial wells (the lowest barrier is +2.6 kcal mol⁻¹). Stabilized adducts (CH₃C·HCH₂OH and CH₃CH(OH)C·H₂) most likely fall apart to reactants at higher temperatures. In all figures the rate coefficients corresponding to the formally direct pathways are shown for the non-abstraction bimolecular products.

In Fig. 8 and 9 the bimolecular product distribution and adduct formation is shown at zero pressure and at 760 Torr, respectively. Addition is significant at 1 atm up to ~1500 K. Allyl radical is by far the most important bimolecular channel, followed by the other direct abstraction products, propen-1-yl and propen-2-yl. Vinyl alcohol, allyl alcohol, and the propenols (*cis*-1-propenol + H, *trans*-1-propenol + H and propen-2-ol + H) are the major non-abstraction bimolecular products, except for low pressures and low temperatures, where acetaldehyde is important. The transition-states leading to acetaldehyde and vinyl alcohol are very close in energy (3.0 and 2.6 kcal mol⁻¹, respectively) and the 0.4 kcal mol⁻¹ difference between the barrier heights is smaller than our cited uncertainties (±1 kcal mol⁻¹), therefore the low-temperature, low-pressure branching between these two species is also uncertain to some extent. The main reason for the acetaldehyde being more significant at lower temperatures is tunneling. The thickness of the Eckart barriers is inversely proportional to the imaginary frequency at the saddle point, and these are very different for the two channels: 533*i* for the vinyl alcohol forming one and 1971*i* for the acetaldehyde forming one. Knowing that the frequency calculation is sensitive to the level of theory used, our low temperature acetaldehyde–vinyl alcohol branching should be treated with caution. The overall rate coefficient at 1 atm between 700 and 1200 K is comparable for the non-abstraction bimolecular products to the rate coefficient for the propen-2-yl + H₂O abstraction channel.

Contrasting our product branching ratios with those of Huynh *et al.*⁶ and Zhou *et al.*⁵ the following can be said. Similar dominance of vinyl alcohol among the non-abstraction bimolecular products was found by Huynh *et al.* (*cf.* Fig. 5 in ref. 6 and Fig. 8 in this article). Their 30 Torr (in Ar bath gas) calculations also show significant amounts of acetaldehyde at low temperatures, as well as acetone; the latter is much smaller in our case. Even though the formation of acetone involves the same initial barrier as for acetaldehyde, the second transition

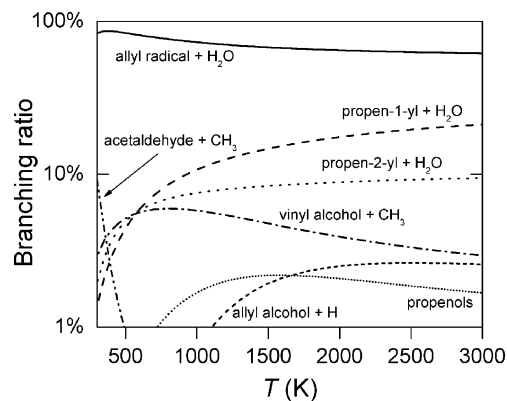


Fig. 8 Calculated branching fractions for the various bimolecular product channels under collisionless conditions.

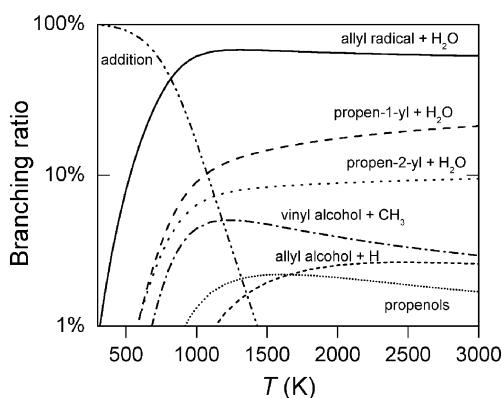


Fig. 9 Calculated branching fractions for the various bimolecular product channels at 760 Torr of He.

state is higher in energy and also tighter. Zhou *et al.* provide the branching fraction at 760 Torr of N_2 diluent, which can be compared to our results presented in Fig. 9. One difference is that addition becomes negligible at ~ 1500 K in our case, while at ~ 1000 K in theirs. This might be because Zhou *et al.* do not use the eigenpairs of the ME to obtain rate coefficients, but the time-dependent populations of the species. This method underestimates the association rate coefficient at higher temperatures, as backdissociation influences the population-time profiles. Another difference is that we do not observe a region where ethenol formation is more dominant than abstraction (allyl radical formation).

It has to be noted that some, but most likely not all of the differences between our and the other calculations arise due to the different electronic structure methods applied. In general, the barrier heights of Zhou *et al.* are lower than ours by 2–4 kcal mol⁻¹, while those of Huynh *et al.* are higher by 2–3 kcal mol⁻¹. Also note that the PES constructed by Huynh *et al.* is likely to produce rate coefficients that are too small at low temperatures, because the inner transition state is too high (+1.5 kcal mol⁻¹). However, they did not attempt to calculate rate coefficients below 500 K.

In Fig. 10–14 the temperature and pressure dependence of the major channels are presented along with the results of the other theoretical calculations. All plots show strong non-Arrhenius character.

Above ~ 150 K strong pressure dependence is observed for addition (Fig. 10), and the overall temperature dependence for addition is negative. Both characteristics are typical of barrierless reactions. Addition leads to stabilization in the two initial wells almost exclusively, since the isomerization barriers are high. The calculated branching between the two wells is very close to 50% at all pressures and temperatures investigated.

Because of the recent interest^{5,6,15,16} in the formation of vinyl alcohol and propenols in flames, we present these rate coefficients along with other calculations in Fig. 11 and 12. These rate coefficients have positive temperature dependence and negative pressure dependence. The temperature dependence of the propenol formation is stronger due to the higher barrier involved in that channel (4.3 kcal mol⁻¹, the barrier for the vinyl alcohol is 2.6 kcal mol⁻¹). The reported values of the other theoretical calculations differ significantly from ours.

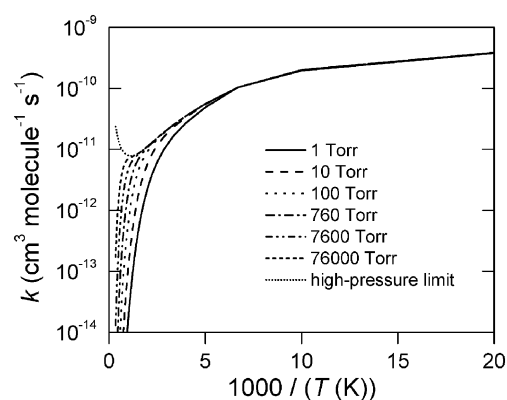


Fig. 10 Arrhenius plot of the addition rate coefficient at various pressures.

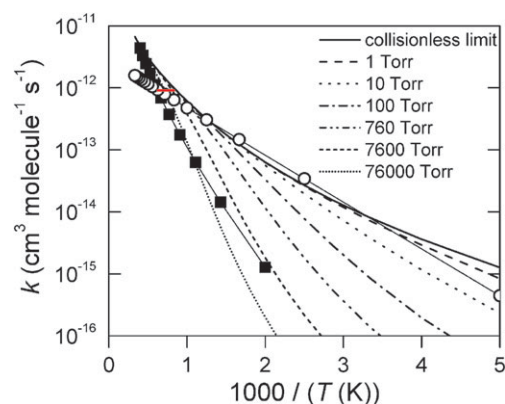


Fig. 11 Arrhenius plot of the vinyl alcohol + CH_3 channel at various pressures. $-\circ-$: calculated values of Zhou *et al.*⁵ for 760 Torr of N_2 ; $-\blacksquare-$: calculated values of Huynh *et al.*⁶ for 30 Torr of Ar. The red horizontal line is the estimated value given by Taatjes *et al.*¹⁶

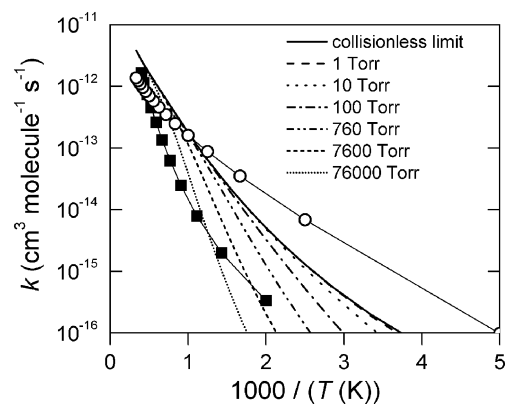


Fig. 12 Arrhenius plot of the propenols + H channels at various pressures. $-\circ-$: calculated values of Zhou *et al.*⁵ for 760 Torr of N_2 ; $-\blacksquare-$: calculated values of Huynh *et al.*⁶ for 30 Torr of Ar.

Interestingly, the high-pressure (760 Torr of N_2) value of Zhou *et al.* is close to our low pressure values, while the low pressure values of Huynh *et al.* (30 Torr Ar) are closer to our high pressure values. One reason for this discrepancy could be the different energy transfer parameters: both studies used the temperature independent value of $\langle \Delta E_d \rangle = 200$ cm⁻¹.

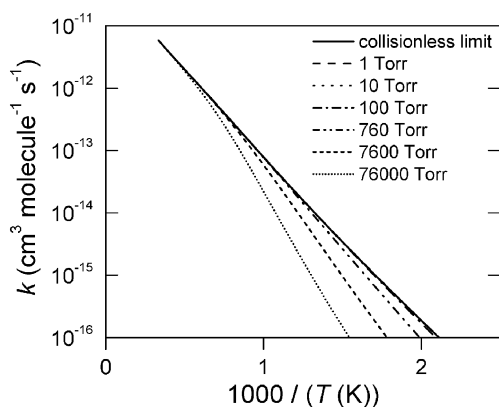


Fig. 13 Arrhenius plot of the allyl alcohol + H channel at various pressures.

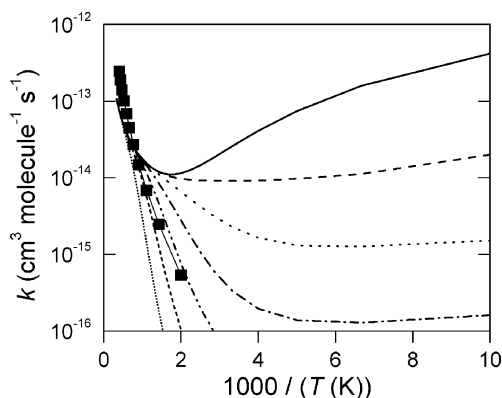


Fig. 14 Arrhenius plot of the acetaldehyde + CH₃ channel at various pressures. Legend for the pressures is the same as in Fig. 13. –○–: calculated values of Huynh *et al.*⁶ for 30 Torr of Ar.

The other, more probable, reason is different barrier heights. As mentioned earlier, Zhou *et al.* have smaller and Huynh *et al.* have higher barriers compared to ours. More specifically, the channel leading to vinyl alcohol has a barrier height of -1.7 kcal mol⁻¹ and 6.5 kcal mol⁻¹, respectively, and the channel leading to propen-2-ol has that of -1.0 kcal mol⁻¹ and 5.0 kcal mol⁻¹, respectively, in these two investigations. Our barrier heights are 2.6 kcal mol⁻¹ and 4.3 kcal mol⁻¹ for vinyl alcohol and propen-2-ol, respectively. Taatjes *et al.*¹⁶ gave a temperature independent estimate for the rate coefficient of vinyl alcohol formation by modeling the measured vinyl alcohol concentration in their flame experiments. This value is also presented in Fig. 11.

For completeness, Fig. 13 and 14 show the Arrhenius plots for the allyl alcohol and acetaldehyde channels. The acetaldehyde formation shows very significant non-Arrhenius behavior. Below ~ 200 K the collisionless rate coefficient levels off or even slightly increases with decreasing temperature. This temperature dependence is due to tunneling, and as discussed before, very sensitive to the level of theory employed to obtain frequencies.

In Fig. 15 the overall rate coefficient (addition + abstraction + non-abstraction bimolecular products) are presented as a function of temperature at different pressures. It has to be

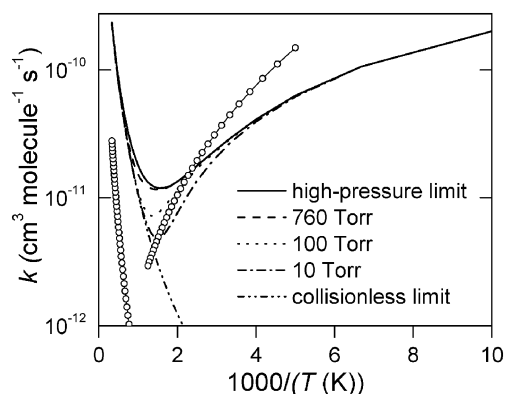


Fig. 15 Temperature dependence of the overall rate coefficient (addition + abstraction + non-abstraction bimolecular channels) at various pressures. –○–: calculated values of Zhou *et al.*⁵

noted that direct comparison of these values to experiments is only possible below ~ 600 K, since backdissociation plays a significant role above this temperature. Zhou *et al.*⁵ provided fitted expressions for the total rate coefficient in two different temperature ranges (200–800 K and 800–3000 K). Again, significant differences exist between their and our results.

In order to facilitate the use of our calculated rate coefficients in atmospheric or combustion models we provide fits to our values. The equilibrium constants for the backdissociation together with the addition rate coefficients are useful for the modeling of propanol oxidation. Double modified-Arrhenius fits are given for the most important channels at various temperatures in Table 2 and are also presented in the ESI in CHEMKIN⁶⁶ format.† Because of the very wide temperature range and the strong non-Arrhenius behavior, we found single modified Arrhenius fits inadequate in most of the cases.

Conclusions

We carried out RRKM-based master equation calculations for the propene + OH reaction and obtained rate coefficients for the various channels in the 50–3000 K temperature and zero to infinite pressure range. RQCISD(T)/cc-pV ∞ Z//B3LYP/6-311++G(d,p) quantum chemical calculations formed the basis of our model. Our effective two transition state model has shown that the association rate for this reaction is determined below ~ 600 K by both the barrierless entrance channel and the submerged barriers following it.

We found remarkable agreement between our calculated rate coefficients and the experimental values available in the literature, and we successfully reproduced the negative temperature dependence at low temperatures as well as the positive temperature dependence at high temperatures. At high temperatures hydrogen abstraction is the major channel, mostly leading to allyl radical. The other important product is vinyl alcohol, recently receiving a lot of attention in combustion systems. Above 1000 K $\sim 5\%$ branching into vinyl alcohol is predicted, necessitating the inclusion of this reaction in comprehensive combustion mechanism.

Table 2 Fitting parameters^a for calculated rate coefficients

Channel	<i>P</i> (He)/atm	<i>A</i> /cm ³ molecule ⁻¹ s ⁻¹	<i>B</i>	<i>C</i> /cal mol ⁻¹	<i>D</i> /cm ³ molecule ⁻¹ s ⁻¹	<i>E</i>	<i>F</i> /cal mol ⁻¹
ABSTRACTION							
Allyl radical + H ₂ O	—	-2.07×10^{-16}	1.73	925	3.12×10^{-17}	2.03	684
Propen-1-yl + H ₂ O	—	1.26×10^{-20}	2.80	2193	1.68×10^{-24}	3.51	-101
Propen-2-yl + H ₂ O	—	7.76×10^{-20}	2.47	1748	9.50×10^{-31}	2.61	-3086
ADDITION goes almost exclusively to the two initial wells (terminal and central addition), with ~50–50% branching. At each pressure the first fit is valid for 50–500 K, while the second for 500–3000 K.							
C ₃ H ₇ O	0.0013	$3.81 \times 10^{+4}$	-5.77	1683	$9.55 \times 10^{+0}$	-4.81	511
		$5.10 \times 10^{+54}$	-20.7	32 402	$1.42 \times 10^{+36}$	-15.84	11 594
	0.01	$3.14 \times 10^{+53}$	-22.2	13 751	1.10×10^{-3}	-3.04	298
		$6.06 \times 10^{+53}$	-20.0	33 874	$1.61 \times 10^{+36}$	-15.51	12 898
	0.013	$1.46 \times 10^{+58}$	-23.70	15 265	6.74×10^{-4}	-2.95	283
		$2.35 \times 10^{+52}$	-19.58	32 874	$6.17 \times 10^{+35}$	-15.34	12 913
	0.025	3.37×10^{-4}	-2.82	263	$2.55 \times 10^{+44}$	-18.83	13 105
		$8.14 \times 10^{+49}$	-18.79	31 361	$5.87 \times 10^{+34}$	-14.93	12 936
	0.1	$2.96 \times 10^{+30}$	-16.59	3552	5.68×10^{-6}	-2.13	127
		$2.29 \times 10^{+44}$	-17.01	27 909	$2.99 \times 10^{+32}$	-14.04	12 945
	0.1315	$1.07 \times 10^{+23}$	-13.62	2834	3.15×10^{-6}	-2.03	106
		$1.60 \times 10^{+43}$	-16.64	27 162	$8.82 \times 10^{+31}$	-13.85	12 887
	1	$2.62 \times 10^{+7}$	-7.311	1324	9.26×10^{-8}	-1.47	-20
		$4.31 \times 10^{+35}$	-14.17	23 079	$3.43 \times 10^{+26}$	-12.04	11 493
	10	$7.82 \times 10^{+4}$	-6.28	1079	2.33×10^{-8}	-1.25	-68
		$1.67 \times 10^{+30}$	-12.23	22 976	$1.42 \times 10^{+18}$	-9.35	8921
	100	$7.82 \times 10^{+4}$	-6.28	1079	2.33×10^{-8}	-1.25	-68
		$3.18 \times 10^{+24}$	-10.23	23 772	$5.08 \times 10^{+8}$	-6.31	6088
	∞	$7.60 \times 10^{+4}$	-6.27	1078	2.17×10^{-8}	-1.24	-71
		2.59×10^{-16}	1.29	-2656	3.93×10^{-19}	2.18	1063
BACKDISSOCIATION this is an equilibrium constant in the same format as the rate coefficients							
Terminal		7.36×10^{-25}	-0.30	-27 414	5.20×10^{-30}	1.43	-28 013
Central		1.02×10^{-23}	-1.10	-28 390	2.17×10^{-30}	1.49	-28 888
BIMOLECULAR the sum of all propene + OH → bimolecular products, except abstraction							
	0	3.51×10^{-18}	1.98	2439	4.49×10^{-10}	-1.73	-214
	0.0013	-8.17×10^{-16}	1.18	1060	3.68×10^{-18}	1.99	484
	0.01	3.54×10^{-18}	1.98	2477	1.46×10^{-20}	1.97	-526
	0.013	4.95×10^{-18}	1.94	2581	1.15×10^{-21}	2.32	-683
	0.025	1.45×10^{-17}	1.81	2926	5.07×10^{-21}	1.97	-589
	0.1	6.70×10^{-16}	1.36	4252	4.17×10^{-25}	3.34	-930
	0.1315	3.26×10^{-15}	1.16	4707	4.91×10^{-28}	4.44	-1217
	1	4.92×10^{-11}	0.00	8132	1.46×10^{-28}	4.76	-223
	10	3.61×10^{-8}	-0.73	12 175	7.36×10^{-29}	4.81	612
	100	7.50×10^{-4}	-1.83	18 784	1.12×10^{-26}	4.25	3044
BIMOLECULAR rate coefficients for selected individual channels							
Allyl alcohol + H	0	-1.31×10^{-9}	-0.45	10 996	3.80×10^{-11}	0.07	10 580
	0.0013	-1.74×10^{-9}	-0.49	11 043	4.43×10^{-11}	0.05	10 611
	0.01	-1.75×10^{-9}	-0.49	11 053	4.57×10^{-11}	0.05	10 623
	0.013	-1.77×10^{-9}	-0.49	11 060	4.77×10^{-11}	0.04	10 634
	0.025	-1.09×10^{-8}	-0.70	11 615	2.64×10^{-10}	-0.16	11 125
	0.1	-1.04×10^{-8}	-0.66	11 794	5.14×10^{-10}	-0.22	11 407
	0.1315	-8.36×10^{-9}	-0.62	11 782	6.27×10^{-10}	-0.24	11 458
	1	1.34×10^{-7}	-1.00	15 339	1.52×10^{-16}	1.42	10 087
	10	2.07×10^{-1}	-2.68	20 993	6.07×10^{-19}	2.14	10 410
	100	$3.45 \times 10^{+1}$	-3.16	26 266	1.36×10^{-21}	2.84	10 481
Vinyl alcohol + CH ₃	0	4.06×10^{-17}	1.55	2310	2.16×10^{-20}	2.11	308
	0.0013	1.11×10^{-16}	1.42	2708	2.14×10^{-18}	1.65	1233
	0.01	6.24×10^{-16}	1.21	3068	3.03×10^{-20}	2.10	1162
	0.013	2.00×10^{-15}	1.06	3326	3.39×10^{-21}	2.48	1128
	0.025	2.70×10^{-14}	0.72	3950	4.78×10^{-22}	2.80	1152
	0.1	3.47×10^{-12}	0.13	5407	2.32×10^{-23}	3.21	1208
	0.1315	8.52×10^{-12}	0.02	5723	1.28×10^{-23}	3.29	1216
	1	1.45×10^{-3}	-2.35	11 290	1.87×10^{-20}	2.50	3238
	10	3.77×10^{-26}	4.03	1952	4.01×10^{-5}	-1.74	13 107
	100	1.08×10^{-1}	-2.58	19 256	5.48×10^{-25}	3.70	3665
Propen-1-ol + H (<i>cis</i> + <i>trans</i>)	0	2.89×10^{-14}	0.69	6864	2.92×10^{-18}	1.57	4133
	0.0013	1.08×10^{-13}	0.53	7292	5.77×10^{-18}	1.53	4288
	0.01	3.77×10^{-14}	0.66	6968	1.79×10^{-17}	1.34	4576
	0.013	3.01×10^{-14}	0.69	6884	1.62×10^{-17}	1.33	4589
	0.025	3.43×10^{-14}	0.68	6899	8.53×10^{-18}	1.36	4594
	0.1	5.20×10^{-13}	0.36	7785	5.20×10^{-19}	1.69	4603

Table 2 (continued)

Channel	P (He)/atm	$A/\text{cm}^3 \text{ molecule}^{-1} \text{ s}^{-1}$	B	$C/\text{cal mol}^{-1}$	$D/\text{cm}^3 \text{ molecule}^{-1} \text{ s}^{-1}$	E	$F/\text{cal mol}^{-1}$
Propen-2-ol + H	0.1315	1.21×10^{-12}	0.26	8071	2.31×10^{-19}	1.80	4603
	1	4.83×10^{-9}	-0.74	11 079	1.71×10^{-22}	2.83	4530
	10	7.49×10^{-5}	-1.86	15 763	5.65×10^{-26}	3.89	4390
	100	6.29×10^{-3}	-2.30	20 501	7.40×10^{-30}	5.03	4132
	0	8.52×10^{-21}	2.42	2447	7.30×10^{-27}	3.67	-518
	0.0013	1.55×10^{-20}	2.35	2635	4.76×10^{-24}	2.92	625
	0.01	6.77×10^{-20}	2.17	3048	8.03×10^{-25}	2.98	704
	0.013	1.07×10^{-19}	2.11	3186	5.19×10^{-25}	3.04	721
	0.025	4.26×10^{-19}	1.94	3598	1.55×10^{-26}	3.62	677
	0.1	2.51×10^{-17}	1.44	4816	7.70×10^{-29}	4.48	687
	0.1315	5.44×10^{-17}	1.35	5084	4.50×10^{-29}	4.56	707
	1	2.58×10^{-14}	0.62	7544	1.27×10^{-30}	5.05	874
	10	2.45×10^{-29}	4.75	2168	4.38×10^{-9}	-0.80	12728
	100	6.40×10^{-5}	-1.85	19 219	8.08×10^{-28}	4.32	4020
Acetaldehyde + CH ₃	0	1.48×10^{-2}	-4.56	464	1.27×10^{-21}	2.24	-1676
	0.0013	-7.37×10^{-17}	0.89	540	1.15×10^{-18}	1.49	-536
	0.01	3.11×10^{-5}	-2.96	4951	9.86×10^{-21}	2.01	-560
	0.013	4.33×10^{-9}	-1.67	3823	1.83×10^{-21}	2.22	-680
	0.025	5.49×10^{-10}	-1.29	3996	1.77×10^{-22}	2.50	-759
	0.1	1.57×10^{-9}	-1.30	5272	1.30×10^{-24}	3.10	-919
	0.1315	2.67×10^{-9}	-1.35	5603	5.09×10^{-25}	3.22	-946
	1	8.58×10^{-8}	-1.67	8264	5.24×10^{-28}	4.05	-1144
	10	8.52×10^{-6}	-2.11	12 359	1.26×10^{-29}	4.49	-680
	100	1.23×10^{-4}	-2.29	17 262	9.05×10^{-29}	4.22	1141

^a $k(T) = A(T/T_0)^B \exp(-C/RT) + D(T/T_0)^E \exp(-F/RT)$, $T_0 = 1 \text{ K}$ and $R = 1.987 \text{ cal K}^{-1} \text{ mol}^{-1}$. *N.B.*: The fitted parameters do not bear any physical meaning. Negative “pre-exponential factors” are unavoidable in certain cases to get a good fit.

Appendix. Rovibronic correction for the partition function of OH

We first consider the uncoupled electronic and rotational partition functions for OH. The uncoupled electronic partition function for OH is given by

$$Q_e(T) = 2(1 + \exp(-E_{SO}/kT)), \quad (\text{A1})$$

where E_{SO} is the spin-orbit splitting of the $^2\Pi_{3/2}$ and $^2\Pi_{1/2}$ states. The uncoupled rotational partition function may be evaluated by approximating OH as a vibrating rotor, *i.e.*,

$$Q_r(T) = \sum_{vj} (2j+1) \exp(-E_{vj}/kT), \quad (\text{A2})$$

$$E_{vj} = B_v j(j+1) - D_v j^2(j+1)^2, \quad (\text{A3})$$

$$B_v = B_e - \alpha_v(v + \frac{1}{2}), \quad (\text{A4})$$

where experimental values of B_e , D_v , and α_v have been previously tabulated for OH.⁶⁷ We do not explicitly consider the vibrational partition function for OH when calculating the rovibronic correction to the OH partition function, and we therefore restrict attention to $v = 0$ in eqn (A2). The uncoupled electronic-rotational partition function is given by the product of eqn (A1) and (A2).

In a more accurate treatment, nuclear rotation is coupled to electronic spin. As discussed by Herzberg,⁶⁷ the electronic-rotational coupling in OH is intermediate of Hund's cases (a) and (b) with rovibronic energy levels given by the two series

$$E_{vj}^1 = B_v \left[\left(j + \frac{1}{2} \right)^2 - \Lambda^2 - \frac{1}{2} \sqrt{4 \left(j + \frac{1}{2} \right)^2 + Y(Y-4)\Lambda^2} \right] - D_v j^4 - E_0 \quad (\text{A5})$$

$$\text{for } j = \frac{3}{2}, \frac{5}{2}, \dots$$

$$E_{vj}^2 = B_v \left[\left(j + \frac{1}{2} \right)^2 - \Lambda^2 + \frac{1}{2} \sqrt{4 \left(j + \frac{1}{2} \right)^2 + Y(Y-4)\Lambda^2} \right] - D_v j^4 - E_0 \quad (\text{A6})$$

$$\text{for } j = \frac{1}{2}, \frac{3}{2}, \dots$$

where E_0 is defined such that $E_{00}^1 = 0$, and $\Lambda = 1$ for $^2\Pi$ OH. The coupled partition function is obtained by summing

$$Q_{e,r}^{\text{coup}}(T) = 2 \sum_{v=0,j} (2j+1) \exp(-E_{vj}^1/kT - E_{vj}^2/kT), \quad (\text{A7})$$

with $v = 0$ to avoid including the vibrational partition function.

In the rate calculations for propene + OH, the rotation was treated using eqn (A2) with $D_v = 0$. (Setting $D_v = 0$ introduces a negligible error in the rotational partition function.) In the uncoupled approximation, the electronic partition function is obtained using (A1). These rates are shown as the unprimed k_{inner} and k_{outer} in eqn (5). In the coupled

Table 3 Electronic, rotational, and coupled partition functions for OH

T/K	Q_e	Q_r	$Q_e Q_r$	$Q_{e,r}^{\text{coup}}$	Q_e^{eff}	Q_e/Q_e^{eff}
0	2.00	1.00	2.00	8.00	8.00	0.25
50	2.04	2.25	4.58	9.82	4.12	0.49
100	2.27	4.11	9.32	14.06	3.42	0.66
200	2.73	7.86	21.48	26.83	3.41	0.80
300	3.02	11.63	35.15	40.91	3.52	0.86
400	3.21	15.40	49.43	55.45	3.60	0.89
500	3.34	19.18	64.02	70.21	3.66	0.91
600	3.43	22.96	78.78	85.11	3.71	0.93
700	3.50	26.76	93.67	100.10	3.74	0.94
800	3.56	30.55	108.64	115.15	3.77	0.94
900	3.60	34.36	123.67	130.26	3.79	0.95
1000	3.64	38.17	138.77	145.41	3.81	0.95
1500	3.75	57.31	214.86	221.69	3.87	0.97
2000	3.81	76.61	291.78	298.75	3.90	0.98
2500	3.85	96.07	369.45	376.51	3.92	0.98
3000	3.87	115.71	447.84	454.99	3.93	0.98
3500	3.89	135.53	526.98	534.21	3.94	0.99
4000	3.90	155.53	606.89	614.19	3.95	0.99

approximation, we define an effective electronic partition function for OH as

$$Q_e^{\text{eff}}(T) = Q_{e,r}^{\text{coup}}/Q_r. \quad (\text{A8})$$

The rate coefficient computed using (A8) is shown as k'_{inner} in eqn (5).

At 0 K, Q_e and Q_e^{eff} differ by a factor of 4 (see Table 3) due to the different degeneracies associated with ground state levels. The correction to the partition function due to electronic-rotational coupling remains significant at room temperature, lowering the partition function by a factor of 0.86. At temperatures above ~ 1000 K, the correction is negligible.

Acknowledgements

The authors thank Yuri Georgievskii for providing the VaReCoF code for the direct VRC-TST calculations. This work is supported by the Division of Chemical Sciences, Geosciences, and Biosciences, the Office of Basic Energy Sciences, the U. S. Department of Energy. Sandia is a multi-program laboratory operated by Sandia Corporation, a Lockheed Martin Company, for the National Nuclear Security Administration under contract DE-AC04-94-AL85000.

References

- 1 M. Szőri, C. Fittschen, I. G. Csizmadia and B. Viskolcz, *J. Chem. Theory Comput.*, 2006, **2**, 1575–1586.
- 2 I. Diaz-Acosta, J. R. Alvarez-Idaboy and A. Vivier-Bunge, *Int. J. Chem. Kinet.*, 1999, **31**, 29–36.
- 3 J. R. Alvarez-Idaboy, I. Diaz-Acosta and A. Vivier-Bunge, *J. Comput. Chem.*, 1998, **19**, 811–819.
- 4 A. M. El-Nahas, T. Uchimaru, M. Sugie, K. Tokuhashi and A. Sekiya, *J. Mol. Struct. (THEOCHEM)*, 2006, **770**, 59–65.
- 5 C.-W. Zhou, Z.-R. Li and X.-Y. Li, *J. Phys. Chem. A*, 2009, **113**, 2372–2382.
- 6 L. K. Huynh, H. R. Zhang, S. Zhang, E. Eddings, A. Sarofim, M. E. Law, P. R. Westmoreland and T. N. Truong, *J. Phys. Chem. A*, 2009, **113**, 3177–3185.
- 7 R. Izsák, M. Szőri, P. J. Knowles and B. Viskolcz, *J. Chem. Theory Comput.*, 2009, **5**, 2313–2321.

- 8 F. P. Tully and J. E. M. Goldsmith, *Chem. Phys. Lett.*, 1985, **116**, 345–352.
- 9 G. P. Smith, P. W. Fairchild, J. B. Jeffries and D. R. Crosley, *J. Phys. Chem.*, 1985, **89**, 1269–1278.
- 10 W. Tsang, *J. Phys. Chem. Ref. Data*, 1991, **20**, 221–273.
- 11 Y. Georgievskii, J. A. Miller and S. J. Klippenstein, *Phys. Chem. Chem. Phys.*, 2007, **9**, 4259–4268.
- 12 C. J. Pope and J. A. Miller, *Proc. Combust. Inst.*, 2000, **28**, 1519–1527.
- 13 J. A. Miller and C. F. Melius, *Combust. Flame*, 1992, **91**, 21–39.
- 14 J. A. Miller, M. J. Pilling and J. Troe, *Proc. Combust. Inst.*, 2005, **30**, 43–88.
- 15 C. A. Taatjes, N. Hansen, A. McIlroy, J. A. Miller, J. P. Senosiain, S. J. Klippenstein, F. Qi, L. S. Sheng, Y. W. Zhang, T. A. Cool, J. Wang, P. R. Westmoreland, M. E. Law, T. Kasper and K. Kohse-Höinghaus, *Science*, 2005, **308**, 1887–1889.
- 16 C. A. Taatjes, N. Hansen, J. A. Miller, T. A. Cool, J. Wang, P. R. Westmoreland, M. E. Law, T. Kasper and K. Kohse-Höinghaus, *J. Phys. Chem. A*, 2006, **110**, 3254–3260.
- 17 W. P. Hess and F. P. Tully, *Chem. Phys. Lett.*, 1988, **152**, 183–189.
- 18 J. R. Dunlop and F. P. Tully, *J. Phys. Chem.*, 1993, **97**, 6457–6464.
- 19 T. Spangenberg, S. Kohler, B. Hansmann, U. Wachsmuth, B. Abel and M. A. Smith, *J. Phys. Chem. A*, 2004, **108**, 7527–7534.
- 20 J. F. Bott and N. Cohen, *Int. J. Chem. Kinet.*, 1991, **23**, 1075–1094.
- 21 T. Klein, I. Barnes, K. H. Becker, E. H. Fink and F. Zabel, *J. Phys. Chem.*, 1984, **88**, 5020–5025.
- 22 R. Zellner and K. Lorenz, *J. Phys. Chem.*, 1984, **88**, 984–989.
- 23 W. S. Nip and G. Paraskevopoulos, *J. Chem. Phys.*, 1979, **71**, 2170–2174.
- 24 A. R. Ravishankara, S. Wagner, S. Fischer, G. Smith, R. Schiff, R. T. Watson, G. Tesi and D. D. Davis, *Int. J. Chem. Kinet.*, 1978, **10**, 783–804.
- 25 A. B. Vakhtin, S. Lee, D. E. Heard, I. W. M. Smith and S. R. Leone, *J. Phys. Chem. A*, 2001, **105**, 7889–7895.
- 26 A. B. Vakhtin, J. E. Murphy and S. R. Leone, *J. Phys. Chem. A*, 2003, **107**, 10055–10062.
- 27 R. Atkinson and J. N. Pitts, *J. Chem. Phys.*, 1975, **63**, 3591–3595.
- 28 V. Schmidt, G. Y. Zhu, K. H. Becker and E. H. Fink, *Ber. Bunsen-Ges. Phys. Chem.*, 1985, **89**, 321–322.
- 29 R. R. Baldwin, M. W. M. Hisham and R. W. Walker, *Proc. Combust. Inst.*, 1984, **20**, 743–750.
- 30 T. J. Wallington, *Int. J. Chem. Kinet.*, 1986, **18**, 487–496.
- 31 I. Barnes, V. Bastian, K. H. Becker, E. H. Fink and W. Nelsen, *J. Atmos. Chem.*, 1986, **4**, 445–466.
- 32 S. Gordon and W. A. Mulac, *Int. J. Chem. Kinet.*, 1975, **1**, 289–299.
- 33 A. M. Winer, A. C. Lloyd, K. R. Darnall and J. N. Pitts, *J. Phys. Chem.*, 1976, **80**, 1635–1639.
- 34 A. M. Winer, A. C. Lloyd, K. R. Darnall, R. Atkinson and J. N. Pitts, *Chem. Phys. Lett.*, 1977, **51**, 221–226.
- 35 R. Atkinson, *J. Phys. Chem. Ref. Data*, 1989, **1**.
- 36 R. Atkinson, D. L. Baulch, R. A. Cox, J. N. Crowley, R. F. Hampson, R. G. Hynes, M. E. Jenkin, M. J. Rossi and J. Troe, *Atmos. Chem. Phys.*, 2006, **6**, 3625–4055.
- 37 K. Hoyermann and R. Sievert, *Ber. Bunsen-Ges. Phys. Chem.*, 1979, **83**, 933–939.
- 38 J. A. Miller and S. J. Klippenstein, *J. Phys. Chem. A*, 2006, **110**, 10528–10544.
- 39 E. E. Greenwald, S. W. North, Y. Georgievskii and S. J. Klippenstein, *J. Phys. Chem. A*, 2005, **109**, 6031–6044.
- 40 E. E. Greenwald, S. W. North, Y. Georgievskii and S. J. Klippenstein, *J. Phys. Chem. A*, 2007, **111**, 5582–5592.
- 41 J. P. Senosiain, S. J. Klippenstein and J. A. Miller, *J. Phys. Chem. A*, 2006, **110**, 6960–6970.
- 42 J. M. L. Martin, *Chem. Phys. Lett.*, 1996, **259**, 669–678.
- 43 D. Feller and D. A. Dixon, *J. Chem. Phys.*, 2001, **115**, 3484–3496.
- 44 J. P. Senosiain, S. J. Klippenstein and J. A. Miller, private communication.
- 45 B. J. Lynch, P. L. Fast, M. Harris and D. G. Truhlar, *J. Phys. Chem. A*, 2000, **104**, 4811–4815.
- 46 M. J. Frisch, G. W. Trucks, H. B. Schlegel, G. E. Scuseria, M. A. Robb, J. R. Cheeseman, J. A. Montgomery, Jr., T. Vreven, K. N. Kudin, J. C. Burant, J. M. Millam, S. S. Iyengar, J. Tomasi, V. Barone, B. Mennucci, M. Cossi, G. Scalmani, N. Rega, G. A. Petersson, H. Nakatsuji, M. Hada,

- M. Ehara, K. Toyota, R. Fukuda, J. Hasegawa, M. Ishida, T. Nakajima, Y. Honda, O. Kitao, H. Nakai, M. Klene, X. Li, J. E. Knox, H. P. Hratchian, J. B. Cross, V. Bakken, C. Adamo, J. Jaramillo, R. Gomperts, R. E. Stratmann, O. Yazyev, A. J. Austin, R. Cammi, C. Pomelli, J. Ochterski, P. Y. Ayala, K. Morokuma, G. A. Voth, P. Salvador, J. J. Dannenberg, V. G. Zakrzewski, S. Dapprich, A. D. Daniels, M. C. Strain, O. Farkas, D. K. Malick, A. D. Rabuck, K. Raghavachari, J. B. Foresman, J. V. Ortiz, Q. Cui, A. G. Baboul, S. Clifford, J. Cioslowski, B. B. Stefanov, G. Liu, A. Liashenko, P. Piskorz, I. Komaromi, R. L. Martin, D. J. Fox, T. Keith, M. A. Al-Laham, C. Y. Peng, A. Nanayakkara, M. Challacombe, P. M. W. Gill, B. G. Johnson, W. Chen, M. W. Wong, C. Gonzalez and J. A. Pople, *GAUSSIAN 03 (Revision C.2)*, Gaussian, Inc., Wallingford, CT, 2004.
- 47 R. D. Amos, A. Bernhardsson, A. Berning, P. Celani, D. L. Cooper, M. J. O. Deegan, A. J. Dobbyn, F. Eckert, C. Hampel, G. Hetzer, P. J. Knowles, T. Korona, R. Lindh, A. W. Lloyd, S. J. McNicholas, F. R. Manby, W. Meyer, M. E. Mura, A. Nicklass, P. Palmieri, R. Pitzer, G. Rauhut, M. Schütz, U. Schumann, H. Stoll, A. J. Stone, R. Tarroni, T. Thorsteinsson and H.-J. Werner, *MOLPRO, a package of ab initio programs designed by H.-J. Werner and P. J. Knowles, Version 2006.1*, 2006.
- 48 S. J. Klippenstein and J. A. Miller, *J. Phys. Chem. A*, 2002, **106**, 9267–9277.
- 49 J. A. Miller and S. J. Klippenstein, *J. Phys. Chem. A*, 2003, **107**, 2680–2692.
- 50 K. S. Pitzer and W. D. Gwinn, *J. Chem. Phys.*, 1942, **10**, 428–440.
- 51 M. J. Assael, T. F. Tsolakis and J. P. M. Trusler, *Thermophysical Properties of Fluids: An Introduction to Their Prediction*, Imperial College Press, London, 1996.
- 52 S. J. Klippenstein, A. F. Wagner, R. C. Dunbar, D. M. Wardlaw, S. H. Robertson and J. A. Miller, VARIFLEX, 2.0m, 2008.
- 53 Y. Georgievskii and S. J. Klippenstein, *J. Chem. Phys.*, 2003, **118**, 5442–5455.
- 54 Y. Georgievskii and S. J. Klippenstein, *J. Phys. Chem. A*, 2003, **107**, 9776–9781.
- 55 Y. Georgievskii and S. J. Klippenstein, VaReCoF, Sandia National Laboratories and Argonne National Laboratory, 2006.
- 56 S. J. Klippenstein, L. R. Khundkar, A. H. Zewail and R. A. Marcus, *J. Chem. Phys.*, 1988, **89**, 4761.
- 57 J. O. Hirschfelder and E. Wigner, *J. Chem. Phys.*, 1939, **7**, 616–628.
- 58 S. N. Rai and D. G. Truhlar, *J. Chem. Phys.*, 1983, **79**, 6046–6059.
- 59 W. J. Chesnavich, L. Bass, T. Su and M. T. Bowers, *J. Chem. Phys.*, 1981, **74**, 2228–2246.
- 60 W. H. Miller, *J. Chem. Phys.*, 1976, **65**, 2216–2223.
- 61 T. J. Lee, A. P. Rendell and P. R. Taylor, *J. Phys. Chem.*, 1990, **94**, 5463–5468.
- 62 T. J. Lee and P. R. Taylor, *Int. J. Quantum Chem.*, 1989, Suppl. 23), 199–207.
- 63 Y. Georgievskii and S. J. Klippenstein, *J. Chem. Phys.*, 2005, **122**, 194103.
- 64 R. X. Fernandes, J. Zador, L. E. Jusinski, C. A. Taatjes and J. A. Miller, *Phys. Chem. Chem. Phys.*, 2009, **11**, 1320–1327.
- 65 A. M. Knepp, G. Meloni, L. E. Jusinski, C. A. Taatjes, C. Cavallotti and S. J. Klippenstein, *Phys. Chem. Chem. Phys.*, 2007, **9**, 4315–4331.
- 66 R. J. Kee, R. M. Rupley, J. A. Miller, M. E. Coltrin, J. F. Grear, E. Meeks, H. K. Moffat, A. E. Lutz, G. Dixon-Lewis, M. D. Smooke, J. Warnatz, G. H. Evans, R. S. Larson, R. E. Mitchell, L. R. Petzold, W. C. Reynolds, M. Caracotsios, W. E. Stewart, P. Glarborg, C. Wang, O. Adigun, W. G. Houf, C. P. Chou, S. F. Miller, P. Ho and D. J. Young, *CHEMKIN-PRO*, Reaction Design, Inc., San Diego, CA, 2008.
- 67 G. Herzberg, *Molecular Spectra and Molecular Structure. I. Spectra of Diatomic Molecules*, Van Nostrand Reinhold, New York, 1950.